

Large-angle production of charged pions by 3 – 12.9 GeV/*c* protons on beryllium, aluminium and lead targets

The HARP Collaboration

M.G. Catanesi¹, E. Radicioni¹, R. Edgecock², M. Ellis^{2,a}, F.J.P. Soler^{2,b}, C. Gößling³, S. Bunyatov⁴, A. Krasnoperov⁴, B. Popov^{4,c}, V. Serdiouk⁴, V. Tereschenko⁴, E. Di Capua⁵, G. Vidal-Sitjes^{5,d}, A. Artamonov^{6,e}, S. Giani⁶, S. Gilardoni⁶, P. Gorbunov^{6,e}, A. Grant⁶, A. Grossheim^{6,f}, A. Ivanchenko^{6,g}, V. Ivanchenko^{6,h}, A. Kayis-Topaksu^{6,i}, J. Panman⁶, I. Papadopoulos⁶, E. Tcherniaev⁶, I. Tsukerman^{6,e}, R. Veenhof⁶, C. Wiebusch^{6,j}, P. Zucchelli^{6,k,l}, A. Blondel⁷, S. Borghi^{7,m}, M.C. Morone^{7,n}, G. Prior^{7,o}, R. Schroeter⁷, C. Meurer⁸, U. Gastaldi⁹, G.B. Mills^{10,p}, J.S. Graulich^{11,q}, G. Grégoire¹¹, M. Bonesini^{12,r}, F. Ferri¹², M. Kirsanov¹³, A. Bagulya¹⁴, V. Grichine¹⁴, N. Polukhina¹⁴, V. Palladino¹⁵, L. Coney^{16,p}, D. Schmitz^{16,p}, G. Barr¹⁷, A. De Santo^{17,s}, F. Bobisut¹⁸, D. Gibin¹⁸, A. Guglielmi¹⁸, M. Mezzetto¹⁸, J. Dumarchez¹⁹, U. Dore²⁰, D. Orestano²¹, F. Pastore²¹, A. Tonazzo²¹, L. Tortora²¹, C. Booth²², L. Howlett²², M. Bogomilov²³, M. Chizhov²³, D. Kolev²³, R. Tsenov²³, S. Piperov²⁴, P. Temnikov²⁴, M. Apollonio²⁵, P. Chimenti²⁵, G. Giannini²⁵, J. Burguet-Castell²⁶, A. Cervera-Villanueva²⁶, J.J. Gómez-Cadenas²⁶, J. Martín-Albo²⁶, P. Novella²⁶, M. Sorel²⁶

¹ Università degli Studi e Sezione INFN, Bari, Italy

² Rutherford Appleton Laboratory, Chilton, Didcot, UK

³ Institut für Physik, Universität Dortmund, Germany

⁴ Joint Institute for Nuclear Research, JINR Dubna, Russia

⁵ Università degli Studi e Sezione INFN, Ferrara, Italy

⁶ CERN, Geneva, Switzerland

⁷ Section de Physique, Université de Genève, Switzerland

⁸ Institut für Physik, Forschungszentrum Karlsruhe, Germany

⁹ Laboratori Nazionali di Legnaro dell' INFN, Legnaro, Italy

¹⁰ Los Alamos National Laboratory, Los Alamos, USA

¹¹ Institut de Physique Nucléaire, UCL, Louvain-la-Neuve, Belgium

¹² Università degli Studi Sezione INFN Milano Bicocca, Piazza Scienza 3, 20126 Milano, Italy

¹³ Institute for Nuclear Research, Moscow, Russia

¹⁴ P.N. Lebedev Institute of Physics (FIAN), Russian Academy of Sciences, Moscow, Russia

¹⁵ Università "Federico II" e Sezione INFN, Napoli, Italy

¹⁶ Columbia University, New York, USA

¹⁷ Nuclear and Astrophysics Laboratory, University of Oxford, UK

¹⁸ Università degli Studi e Sezione INFN, Padova, Italy

¹⁹ LPNHE, Universités de Paris VI et VII, Paris, France

²⁰ Università "La Sapienza" e Sezione INFN Roma I, Roma, Italy

²¹ Università degli Studi e Sezione INFN Roma III, Roma, Italy

²² Dept. of Physics, University of Sheffield, UK

²³ Faculty of Physics, St. Kliment Ohridski University, Sofia, Bulgaria

²⁴ Institute for Nuclear Research and Nuclear Energy, Academy of Sciences, Sofia, Bulgaria

²⁵ Università degli Studi e Sezione INFN, Trieste, Italy

²⁶ Instituto de Física Corpuscular, IFIC, CSIC and Universidad de Valencia, Spain

Received: 13 November 2007 /

Published online: 12 January 2008 – © Springer-Verlag / Società Italiana di Fisica 2008

Abstract. Measurements of the double-differential π^\pm production cross-section in the range of momentum $100 \text{ MeV}/c \leq p < 800 \text{ MeV}/c$ and angle $0.35 \text{ rad} \leq \theta < 2.15 \text{ rad}$ in proton–beryllium, proton–aluminium and proton–lead collisions are presented. The data were taken with the HARP detector in the T9 beam line of the CERN PS. The pions were produced by proton beams in a momentum range from 3 GeV/c to 12.9 GeV/c hitting a target with a thickness of 5% of a nuclear interaction length. The tracking and identification of the produced particles was performed using a small-radius cylindrical time projection chamber (TPC) placed inside a solenoidal magnet. Incident particles were identified by an elaborate system of beam detectors. Results are obtained for the double-differential cross-sections $d^2\sigma/dpd\theta$ at six incident proton beam momenta (3 GeV/c, 5 GeV/c, 8 GeV/c, 8.9 GeV/c (Be only), 12 GeV/c and 12.9 GeV/c (Al only)) and compared to previously available data.

1 Introduction

The HARP experiment [1] makes use of a large-acceptance spectrometer for systematic study of the hadron production on a large range of target nuclei for beam momenta from 1.5 to 15 GeV/c. The main motivations are to measure pion yields for a quantitative design of the proton driver of a future neutrino factory [2, 3], to provide measurements to allow substantially improved calculations of the atmospheric neutrino flux [4–8] to be made and to measure particle yields as input for the flux calculation of accelerator neutrino experiments, such as K2K [9, 10], MiniBooNE [11, 12] and SciBooNE [13].

Measurements of the double-differential cross-section, $d^2\sigma/\text{dpd}\theta$ for π^\pm production at large angles by protons of 3 GeV/c, 5 GeV/c, 8 GeV/c, 8.9 GeV/c (Be only), 12 GeV/c and 12.9 GeV/c (Al only) momentum impinging on a thin beryllium, aluminium or lead target of 5% nuclear interaction length (λ_I) are presented. These measurements are of special interest for target materials used in conventional accelerator neutrino beams (Be, Al) and in neutrino factory designs (Pb).

In this energy range and for these nuclear targets, only very sparse data sets are available from previous experi-

ments, usually with large uncertainties [14, 15], aside what has been published in [16, 17].

Results for other nuclei, such as Be, Al for pions produced in the forward direction and C, Cu, Sn, Ta for pion production at large angles are presented in different HARP publications [18–21]. HARP is the first experiment to provide a large data set taken with many different targets, full particle identification and large detector acceptance down to low secondary momentum ($\simeq 200 \text{ MeV}/c$). This paper completes the range of solid target materials for which HARP data are available. The combination of the data sets make it possible to perform systematic comparisons of hadron production models with measurements at different incoming beam momenta over a large range of target atomic number A .

Data were taken in the T9 beam of the CERN PS. About 3.1×10^5 , 5.1×10^5 , 1.6×10^5 well-reconstructed secondary pion tracks for the beryllium, aluminium and lead targets were selected from 1.6, 2.3 and 0.9 millions of incoming protons, which gave an interaction trigger in the large angle spectrometer.

The analysis proceeds by selecting tracks in the time projection chamber (TPC) in events with incident beam protons. Momentum and polar angle measurements and particle identification are based on the measurements of track position and energy deposition in the TPC. An unfolding method is used to correct for experimental resolution, efficiency and acceptance and to obtain the double-differential pion production cross-sections. The method allows a full error evaluation to be made. The analysis follows closely the methods used for the determination of π^\pm production by protons on a tantalum target which are fully described in [21] and will be only briefly outlined here. A comparison with available data is presented.

2 Experimental apparatus and data analysis

The HARP detector is shown in Fig. 1 and is fully described in [23, 24]. The forward spectrometer, mainly used in the particle production analysis for the conventional neutrino beams and atmospheric neutrino flux, comprises a dipole magnet, large planar drift chambers (NDC) [25], a time-of-flight wall (TOFW) [26, 27], a threshold Cherenkov counter (CHE) and an electromagnetic calorimeter (ECAL). In the large-angle region of particle production a cylindrical TPC with a radius of

^a Now at FNAL, Batavia, Illinois, USA.

^b Now at University of Glasgow, UK.

^c Also supported by LPNHE, Paris, France.

^d Now at Imperial College, University of London, UK.

^e ITEP, Moscow, Russian Federation.

^f Now at TRIUMF, Vancouver, Canada.

^g On leave of absence from Novosibirsk State University, Russia.

^h On leave of absence from Ecoanalitica, Moscow State University, Moscow, Russia.

ⁱ Now at Çukurova University, Adana, Turkey.

^j Now at III Phys. Inst. B, RWTH Aachen, Aachen, Germany.

^k Now at SpinX Technologies, Geneva, Switzerland.

^l On leave of absence from INFN, Sezione di Ferrara, Italy.

^m Now at CERN, Geneva, Switzerland.

ⁿ Now at University of Rome Tor Vergata, Italy.

^o Now at Lawrence Berkeley National Laboratory, Berkeley, California, USA.

^p MiniBooNE Collaboration.

^q Now at Section de Physique, Université de Genève, Switzerland, Switzerland.

^r e-mail: maurizio.bonesini@mib.infn.it

^s Now at Royal Holloway, University of London, UK.

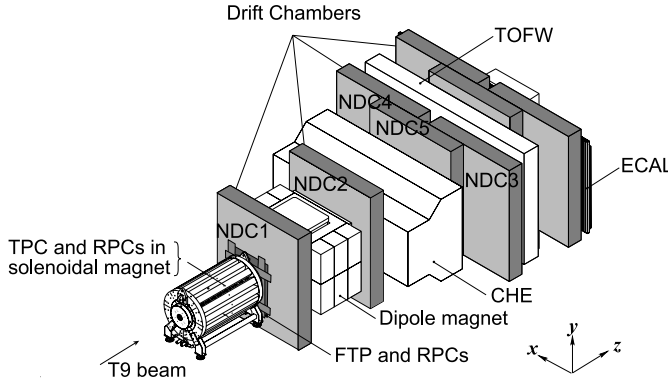


Fig. 1. Schematic layout of the HARP detector. The convention for the coordinate system is shown in the *lower-right corner*. The three most downstream (unlabelled) drift chamber modules are only partly equipped with electronics and are not used for tracking

408 mm (active region) is positioned inside a solenoidal magnet with a field of 0.7 T. The TPC detector was designed to measure and identify tracks in the angular region from 0.25 to 2.5 rad with respect to the beam axis. The target is placed inside the inner field cage (IFC) of the TPC such that, in addition to particles produced in the forward direction, backward-going tracks can be measured. The targets have a nominal thickness of 5% λ_I and a cylindrical shape with a nominal diameter of 30 mm and each of the three targets have a purity above 99.95%. The Be, Al and Pb targets have a thickness of 20.46 mm, 19.80 mm and 8.37 mm with a measured variation of less than ± 0.02 mm, ± 0.07 mm and ± 0.08 mm, respectively.

The TPC is used for tracking, momentum determination and the measurement of the energy deposition dE/dx for particle identification [28]. A set of resistive plate chambers (RPC) form a barrel inside the solenoid around the TPC to measure the arrival time of the secondary particles [29–31]. Charged particle identification (PID) can be achieved by measuring the ionization per unit length in the gas (dE/dx) as a function of the total momentum of the particle. Additional PID can be performed through a time-of-flight measurement with the RPCs.

The momentum of the T9 beam is known with a precision of the order of 1% [32–34]. The absolute normalization of the number of incident protons was performed using a total of 1 148 120 incident proton triggers. These are triggers where the same selection on the beam particle was applied but no selection on the interaction was performed. The rate of this trigger was down-scaled by a factor 64. A cross-check of the absolute normalization was provided by counting tracks in the forward spectrometer.

Beam instrumentation provides identification of the incoming particle, the determination of the time when it hits the target, and the impact point and direction of the beam particle on the target. It is based on a set of four multi-wire proportional chambers (MWPC) to measure position and direction of the incoming beam particles and time-of-flight detectors and N_2 -filled Cherenkov counters to identify incoming particles. Several trigger detectors are in-

stalled to select events with an interaction and to define the normalization.

The beam of positive particles used for this measurement contains mainly positrons, pions and protons, with small components of kaons and deuterons and heavier ions. The proton fraction in the incoming beam varies from 35% at 3 GeV/c to 92% at 12 GeV/c. The length of the accelerator spill is 400 ms with a typical intensity of 15 000 beam particles per spill.

In addition to the usual need for calibration of the detector, a number of hardware shortfalls, discovered mainly after the end of data-taking, had to be overcome to use the TPC data reliably in the analysis. The TPC is affected by a relatively large number of dead or noisy pads and static and dynamic distortions of the reconstructed trajectories. Static distortions are caused by the inhomogeneity of the electric field, due to an accidental mismatch between the inner and outer field cage (powered by two distinct HV supplies) and other sources. Dynamic distortions are caused instead by the build-up of ion-charge density in the drift volume during the 400 ms long beam spill. All these effects were fully studied and available corrections are described in detail in [21]. While methods to correct the dynamic distortions of the TPC tracks are being developed, a practical approach has been followed in the present analysis. Only the events corresponding to the early part of the spill, where the effects of the dynamic distortions are still small, have been used.¹ The time interval between spills is large enough to drain all charges in the TPC related to the effect of the beam. The combined effect of the distortions on the kinematic quantities used in the analysis has been studied in detail and only that part of the data for which the systematic errors can be assessed with physical benchmarks was used, as explained in [21]. More than 30% of the recorded data can thus be used in the current analysis.

The absolute momentum scale is determined by using elastic scattering events off a hydrogen target. The angle of the forward scattered particle is used to predict the momentum of the recoil proton, to be compared to the one measured by the TPC. To study the stability of this measurement protons are selected in a narrow band with a relatively large dE/dx where dE/dx depends strongly on momentum. The average momentum for the selected protons remains stable within 3% as a function of time-in-spill over the part of the spill used in this analysis.

The delicate issue of the TPC momentum scale is fully addressed in a dedicated paper [22]. Only a short outline of the data analysis is presented here, for more details see [21].

The analysis proceeds by first selecting a beam proton hitting the target, not accompanied by other tracks. Then an event is required to give a large angle interaction (LAI) trigger to be retained. After the event selection the sample of tracks to be used for analysis is defined. At least twelve space points in the TPC out of a maximum of twenty are required to consider a track. This cut ensures a good measurement of the track parameters and the dE/dx . For the

¹ This translates into a cut on the maximum number of events (N_{evt}) to be retained.

Table 1. Total number of events and tracks used in the beryllium, aluminium and lead 5% λ_I target data sets, and the number of protons on target as calculated from the pre-scaled trigger count. For each entry the first line shows beryllium target data, the second line – aluminium target data and the third (last) line – lead target data

Data set (GeV/c)		3	5	8	8.9	12	12.9
Total DAQ events	(Be)	1 409 710	1 705 362	2 010 031	3 969 685	1 288 354	–
	(Al)	1 586 331	1 094 308	1 706 919	–	619 021	6 644 256
	(Pb)	1 299 264	2 234 984	1 949 950	–	630 417	–
Acc. protons with LAI	(Be)	77 223	182 423	365 500	692 150	300 939	–
	(Al)	69 794	120 948	341 687	–	71 554	1 715 323
	(Pb)	79 188	207 004	415 982	–	188 134	–
Fraction of triggers used (N_{evt} cut)	(Be)	35%	33%	36%	41%	41%	–
	(Al)	48%	40%	33%	–	42%	35%
	(Pb)	36%	32%	36%	–	27%	–
π^- selected with PID	(Be)	3120	11 168	29 337	63 887	29 506	–
	(Al)	3882	9233	27 809	–	19 290	168 229
	(Pb)	2347	11 842	42 576	–	18 092	–
π^+ selected with PID	(Be)	5520	15 331	37 049	78 727	35 136	–
	(Al)	6396	13 045	35 991	–	23 440	203 924
	(Pb)	3203	13 318	46 150	–	19 040	–

selected tracks a cut on d'_0 (the distance of closest approach to the extrapolated trajectory of the incoming beam particle in the plane perpendicular to the beam direction) and z'_0 (the z-coordinate where the distance of the secondary track and the beam track is minimal) is applied. Finally, only tracks with $100 \text{ MeV}/c \leq p \leq 800 \text{ MeV}/c$ and $p_T \geq 55 \text{ MeV}/c$ are accepted.

Table 1 shows the number of events and the number of π^\pm selected in the p –Be, p –Al and p –Pb analysis. The total number of events taken by the data acquisition (“Total DAQ events”) includes trigger of all types as well as calibration events. The number of accepted events for the analysis (“Accepted protons with LAI”) is obtained from incoming protons in coincidence with a large angle trigger. The large difference between the two numbers is due to the relatively large fraction of pions in the beam and to the larger number of triggers taken for the measurements with the forward dipole spectrometer. These data will be the subject of other publications. The fraction of data used for the analysis (“Fraction of triggers used”) after a cut on the maximum event number to be retained in the spill (“ N_{evt} cut”) to avoid dynamic distortion corrections is then reported. Finally, the rows “Negative particles”, “Positive particles”, “ π^- selected with PID” and “ π^+ selected with PID” show the number of accepted tracks with negative and positive charge and the ones passing in addition the pion PID criteria, respectively.

3 Experimental results

The double-differential cross-section for the production of a particle of type α can be expressed in the laboratory system as:

$$\frac{d^2\sigma_\alpha}{dp_i d\theta_j} = \frac{1}{N_{\text{pot}}} \frac{A}{N_A \rho t} \sum_{i',j',\alpha'} M_{ij\alpha i' j' \alpha'}^{-1} N_{i' j'}^{\alpha'}, \quad (1)$$

where $\frac{d^2\sigma_\alpha}{dp_i d\theta_j}$ is expressed in bins of true momentum (p_i), angle (θ_j) and particle type (α). The factor $\frac{A}{N_A \rho t}$ in (1) is the inverse of the number of target nuclei per unit area (A is the atomic mass, N_A is the Avogadro number, ρ and t are the target density and thickness).²

The ‘raw yield’ $N_{i' j'}^{\alpha'}$ is the number of particles of observed type α' in bins of reconstructed momentum ($p_{i'}$) and angle ($\theta_{j'}$). These particles must satisfy the event, track and PID selection criteria. Although, thanks to the stringent PID selection, the background from misidentified protons in the pion sample is small, the pion and proton raw yields ($N_{i' j'}^{\alpha'}$, for $\alpha' = \pi^-, \pi^+, p$) have been measured simultaneously. It is thus possible to correct for the small remaining proton background in the pion data without prior assumptions concerning the proton production cross-section.

The matrix $M_{ij\alpha i' j' \alpha'}^{-1}$ corrects for the efficiency and resolution of the detector. It unfolds the true variables $i j \alpha$ from the reconstructed variables $i' j' \alpha'$ with a Bayesian technique [35] and corrects the observed number of particles to take into account effects such as trigger efficiency, reconstruction efficiency, acceptance, absorption, pion decay, tertiary production, PID efficiency, PID misidentification and electron background. The method used to correct for the various effects is described in more detail in [21].

In order to predict the population of the migration matrix element $M_{ij\alpha i' j' \alpha'}$, the resolution, efficiency and acceptance of the detector are obtained from the Monte Carlo. This is accurate provided that the Monte Carlo simulation describes these quantities correctly. Where some deviations from the control samples measured from the data are found, the data are used to introduce (small) corrections to the Monte Carlo. Using the unfolding ap-

² We do not make a correction for the attenuation of the proton beam in the target, so that the cross-sections are strictly valid for a $\lambda_I = 5\%$ target.

proach, possible known biases in the measurements are taken into account automatically as long as they are described by the Monte Carlo. In the experiment simulation, which is based on the GEANT4 toolkit [36], the materials in the beam-line and the detector are accurately described as well as the relevant features of the detector response and the digitization process. In general, the Monte Carlo simulation compares well with the data, as shown in [21].

The result is normalized to the number of incident protons on target N_{pot} . The absolute normalization of the result is calculated in the first instance relative to the number of incident beam particles accepted by the selection. After unfolding, the factor $\frac{A}{N_{\text{Apot}}}$ is applied. The beam normalization using down-scaled incident proton triggers has uncertainties smaller than 2% for all beam momentum settings.

The background due to interactions of the primary protons outside the target (called ‘Empty target background’) is measured using data taken without the target mounted in the target holder. Owing to the selection criteria which only accept events from the target region and the good definition of the interaction point this background is negligible ($< 10^{-5}$). The background of interactions of the primary proton outside the target can be suppressed for large angle tracks measured in the TPC owing to the good resolution in z . This is contrary to the situation in the forward spectrometer where an interaction in the target cannot be

distinguished from an interaction in upstream or downstream material [18, 19].

The effects of these uncertainties on the final results are estimated by repeating the analysis with the relevant input modified within the estimated uncertainty intervals. In many cases this procedure requires the construction of a set of different migration matrices. The correlations of the variations between the cross-section bins are evaluated and expressed in the covariance matrix. Each systematic error source is represented by its own covariance matrix. The sum of these matrices describes the total systematic error.

3.1 Cross-section measurements

The measured double-differential cross-sections for the production of π^+ and π^- in the laboratory system as a function of the momentum and the polar angle for each incident beam momentum are shown in Figs. 2–4 for Be, Al and Pb, respectively. The error bars shown are the square-roots of the diagonal elements in the covariance matrix, where statistical and systematic uncertainties are combined in quadrature. Correlations cannot be shown in the figures. The correlation of the statistical errors (introduced by the unfolding procedure) are typically smaller than 20%

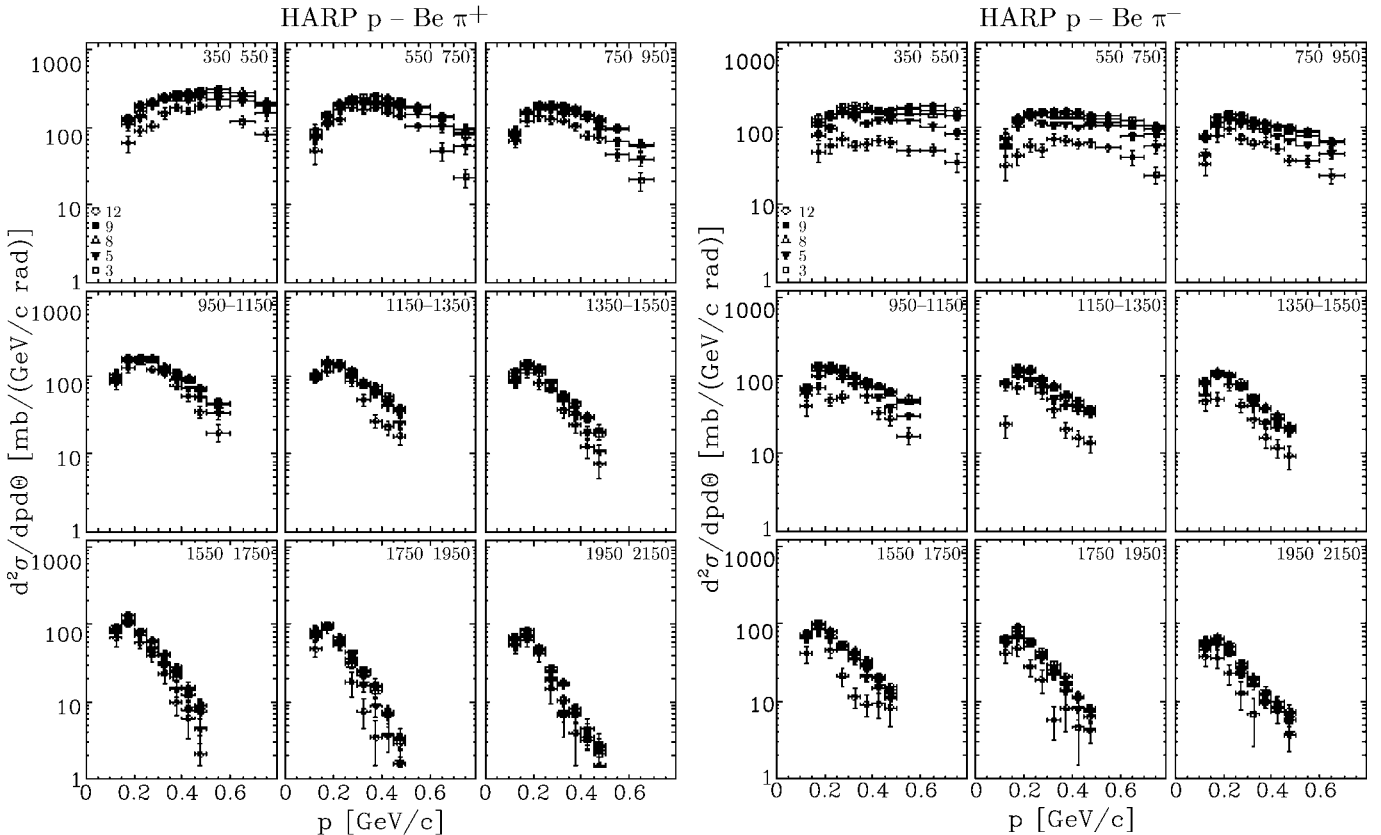


Fig. 2. Double-differential cross-sections for π^+ production (left) and π^- production (right) in p -Be interactions as a function of momentum displayed in different angular bins (shown in mrad in the panels). The error bars represent the combination of statistical and systematic uncertainties

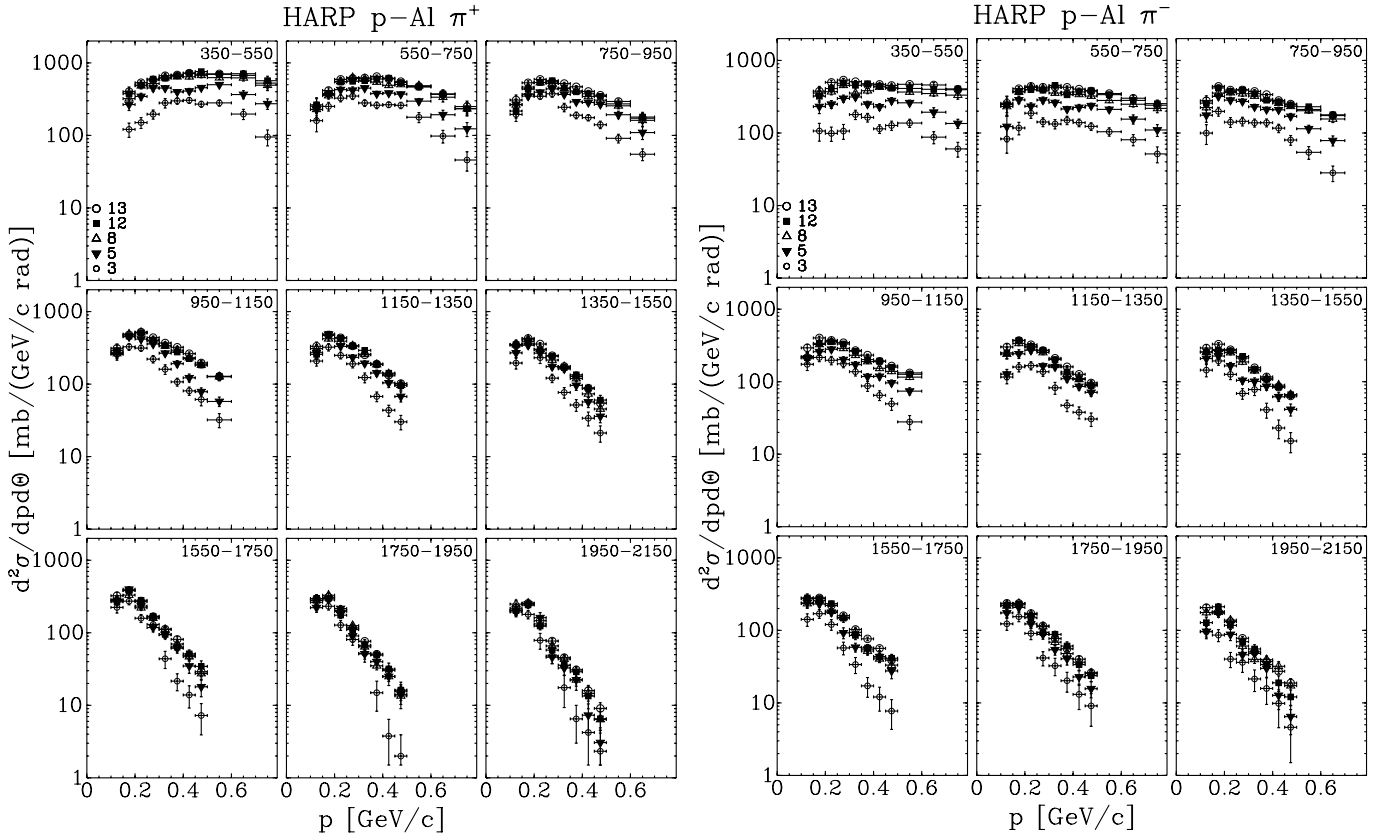


Fig. 3. Double-differential cross-sections for π^+ production (left) and π^- production (right) in p -Al interactions as a function of momentum displayed in different angular bins (shown in mrad in the panels). The error bars represent the combination of statistical and systematic uncertainties. In the figure, the symbol legend 13 (9) refers to 12.9 (8.9) GeV/c nominal beam momentum

for adjacent momentum bins and even smaller for adjacent angular bins. The correlations of the systematic errors are larger, typically 80% for adjacent bins. The overall scale error is not shown. The latter error is 2% for Be and Al and 3% for Pb due to the larger variation in the measured thickness of the lead target. The results of this analysis are also tabulated in the Appendix.

To better visualize the dependence on the incoming beam momentum, the same data averaged over the angular range (for the forward going and backward going tracks) covered by the analysis are shown separately for π^+ and π^- in Fig. 5. The spectrum of pions produced in the backward direction is much steeper than that in the forward direction. The increase of the pion yield per proton is visible in addition to a change of spectrum towards higher momentum of the secondaries produced by higher momentum beams in the forward direction. This dependence is much weaker for Be than for Pb.

The dependence of the integrated pion yields on the incident beam momentum is shown in Fig. 6 and compared with previous results obtained with the same apparatus. The π^+ and π^- yields are integrated over the region $0.350 \text{ rad} \leq \theta < 0.950 \text{ rad}$ and $100 \text{ MeV}/c \leq p < 700 \text{ MeV}/c$. Whereas the beam energy dependence of the yields in the p -C, p -Be data differs clearly from the dependence in the p -Ta, p -Pb data one can observe that the p -Al, p -Cu and p -Sn data display a smooth tran-

sition between them. The dependence in the p -C, p -Be data is much more flat with a saturation of the yield between 8 GeV/c and 12 GeV/c with the p -Al, p -Cu and p -Sn showing an intermediate behaviour.

The integrated π^-/π^+ ratio in the forward direction is displayed in Fig. 7 as a function of secondary momentum. In the covered part of the momentum range in most bins more π^+ 's are produced than π^- 's. The π^-/π^+ ratio has features similar to the ones observed in our p -C [20] and p -Ta data [21]. In the p -Pb data the ratio is closer to unity than for the p -Be, p -Al data. In the lead data a similar effect is observed as in the previously published tantalum data, namely that the number of π^+ 's produced is smaller than the number of π^- 's in the lowest momentum bin (100–150 MeV/c) for the 8 GeV/c and 12 GeV/c incoming beam momenta. A similar effect was seen by E910 in their p -Au data [16]. Lower- A targets do not show this behaviour.

The dependence of the integrated pion yields on the atomic number A is shown in Fig. 8 combining the results with the p -Ta data [21], the p -C data and the p -Cu, p -Sn data [20] taken with the same apparatus and analysed using the same methods. The π^+ yields integrated over the region $0.350 \text{ rad} \leq \theta < 1.550 \text{ rad}$ and $100 \text{ MeV}/c \leq p < 700 \text{ MeV}/c$ are shown in the left panel and the π^- data integrated over the same region in the right panel for four different beam momenta. One observes a smooth behaviour of

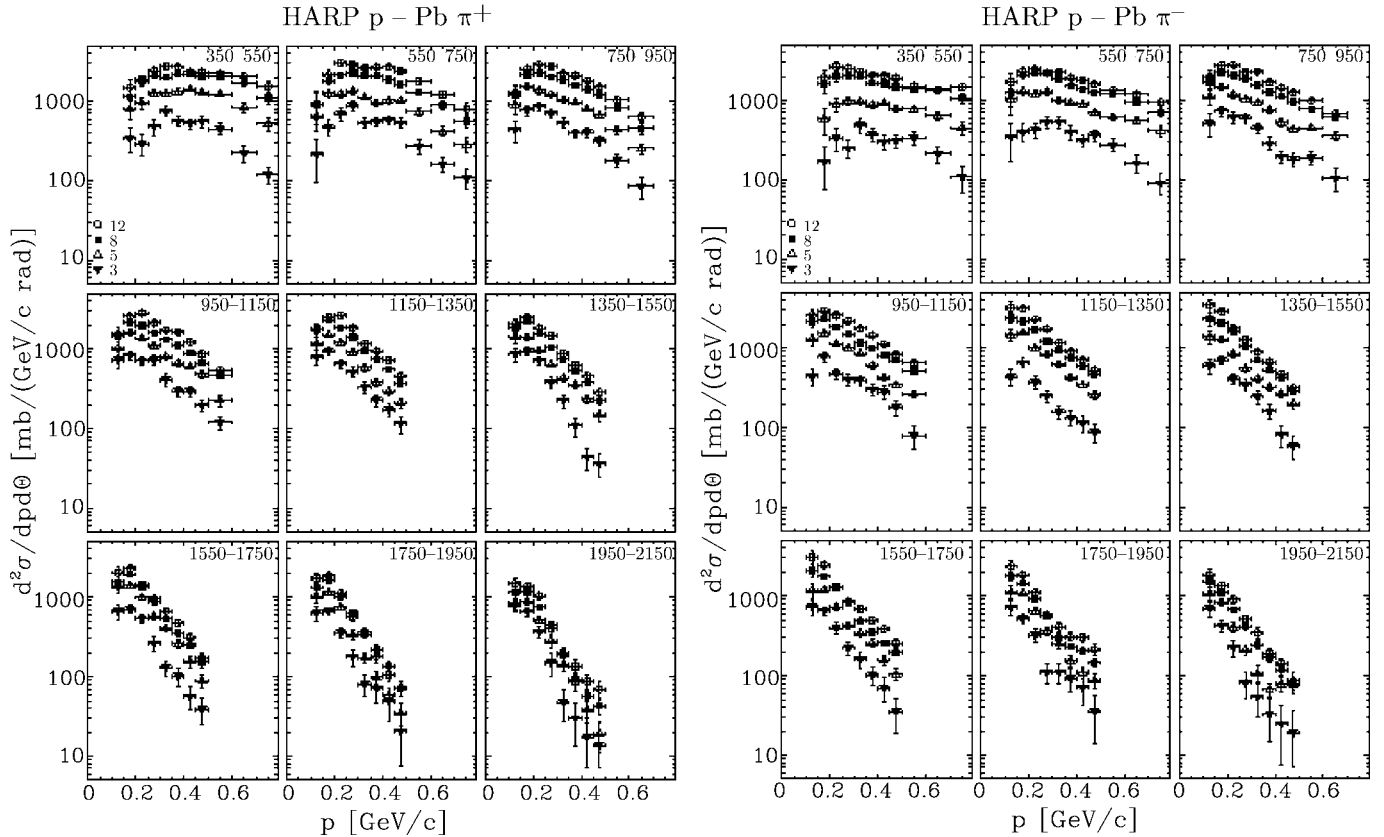


Fig. 4. Double-differential cross-sections for π^+ production (*left*) and π^- production (*right*) in p -Pb interactions as a function of momentum displayed in different angular bins (shown in mrad in the panels). The *error bars* represent the combination of statistical and systematic uncertainties

the integrated yields. The A -dependence is slightly different for π^- and π^+ production, the latter saturating earlier, especially at lower beam momenta.

The experimental uncertainties are summarized in Table 2. One observes that only for the 3 GeV/c beam the statistical error is similar in magnitude to the systematic error, while the statistical error is negligible for the 8 GeV/c and 12 GeV/c beam settings. The statistical error is calculated by error propagation as part of the unfolding procedure. It takes into account that the unfolding matrix is obtained from the data themselves³ and hence contributes also to the statistical error. This procedure almost doubles the statistical error, but avoids an important systematic error which would otherwise be introduced by assuming a cross-section model *a priori* to calculate the corrections.

The largest systematic error corresponds to the uncertainty in the absolute momentum scale, which was estimated to be around 3% using elastic scattering [21, 22]. At low momentum in the relatively small angle forward direction the uncertainty in the subtraction of the electron and positron background due to π^0 production is dom-

inant ($\sim 6\%-10\%$). This uncertainty is split between the variation in the shape of the π^0 spectrum and the normalization using the identified electrons. The target region definition and the uncertainty in the PID efficiency and background from tertiaries (particles produced in secondary interactions) are of similar size and are not negligible ($\sim 2\%-3\%$). Relatively small errors are introduced by the uncertainties in the absorption correction, absolute knowledge of the angular and the momentum resolution. The correction for tertiaries is relatively large at low momenta and large angles ($\sim 3\%-5\%$). As expected, this region is most affected by this component. The errors are quoted for the positive pion data. Owing to the similarity of the spectra the errors are very similar for the negative pions.

As already mentioned above, the overall normalization has an uncertainty of 2% for Be and Al and 3% for Pb, and is not reported in the table. It is mainly due to the uncertainty in the efficiency that beam protons counted in the normalization actually hit the target, with smaller components from the target thickness and density and beam particle counting procedure.

The Pb data presented in this paper are particularly relevant for the design of the input stage of future neutrino factories. This experiment covers the full momentum range of interest for production angles above 0.35 rad. When one defines the effective coverage of the kinematic range as

³ The migration matrix is calculated without prior knowledge of the cross-sections, while the unfolding procedure determined the unfolding matrix from the migration matrix and the distributions found in the data.

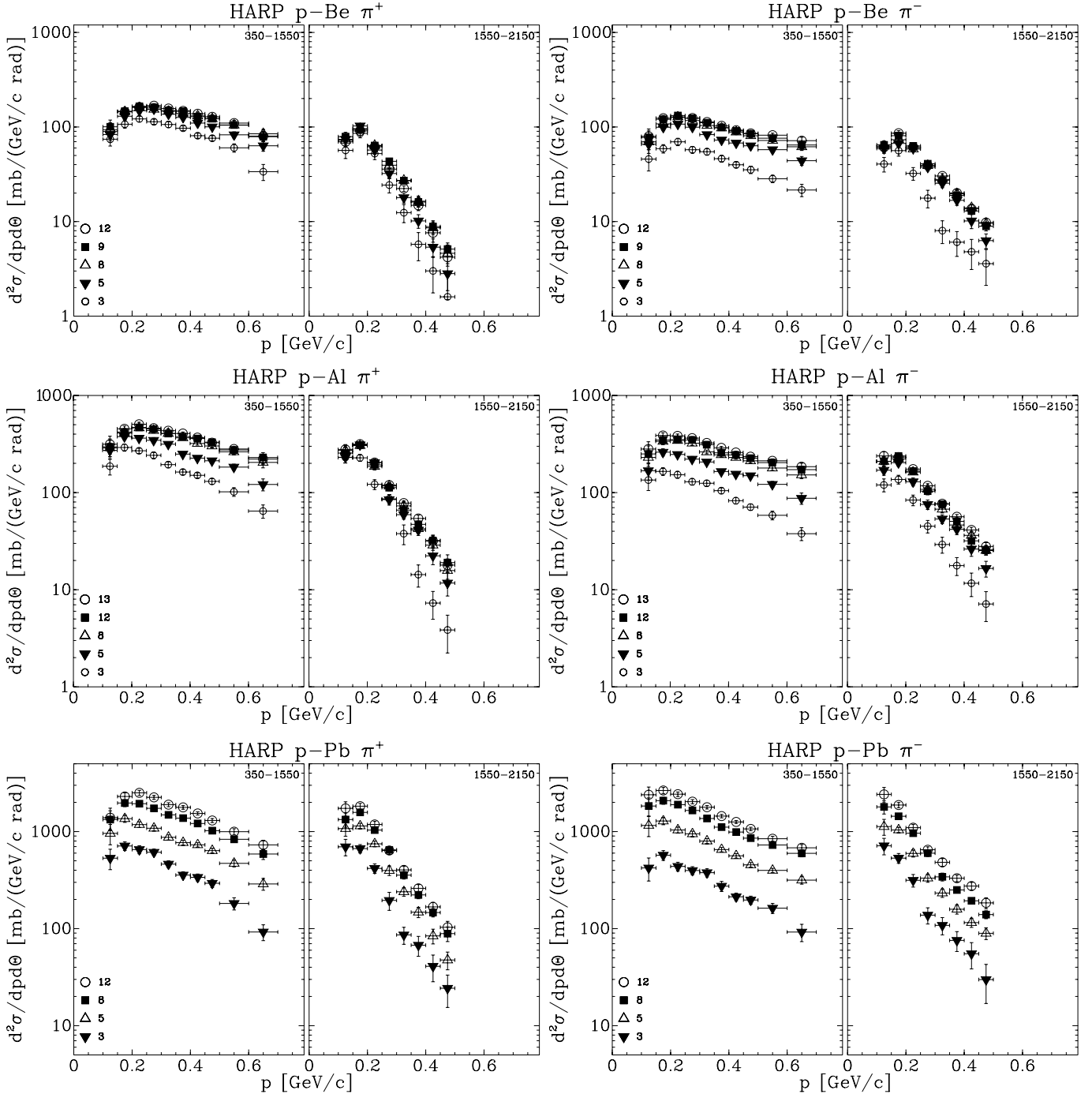


Fig. 5. Double-differential cross-sections for π^+ and π^- production in $p\text{-Be}$ (top), $p\text{-Al}$ (middle) and $p\text{-Pb}$ (bottom) interactions as a function of momentum averaged over the angular region covered by this experiment (shown in mrad). The left panel of each pair shows forward production ($350 \text{ mrad} \leq \theta < 1550 \text{ mrad}$), while the right panel of each pair shows backward production ($1550 \text{ mrad} \leq \theta < 2150 \text{ mrad}$). The error bars obtained after summing the bins of the double-differential cross-sections take into account the correlations of the statistical and systematic uncertainties. In the figure, the symbol legend 13 (9) refers to 12.9 (8.9) GeV/c nominal beam momentum

the fraction of muons transported by the input stage of a neutrino factory design originating from decays for which the pion production cross-section is within the kinematic range measured by the present experiment then one evaluates this effective coverage to be close to 70% [37, 38],

using a particular model for pion production at an incoming beam momentum of 10.9 GeV/c [39] for the ISS input stage [40, 41].

The π^+ and π^- production cross-sections were integrated over the full HARP kinematic range in the forward

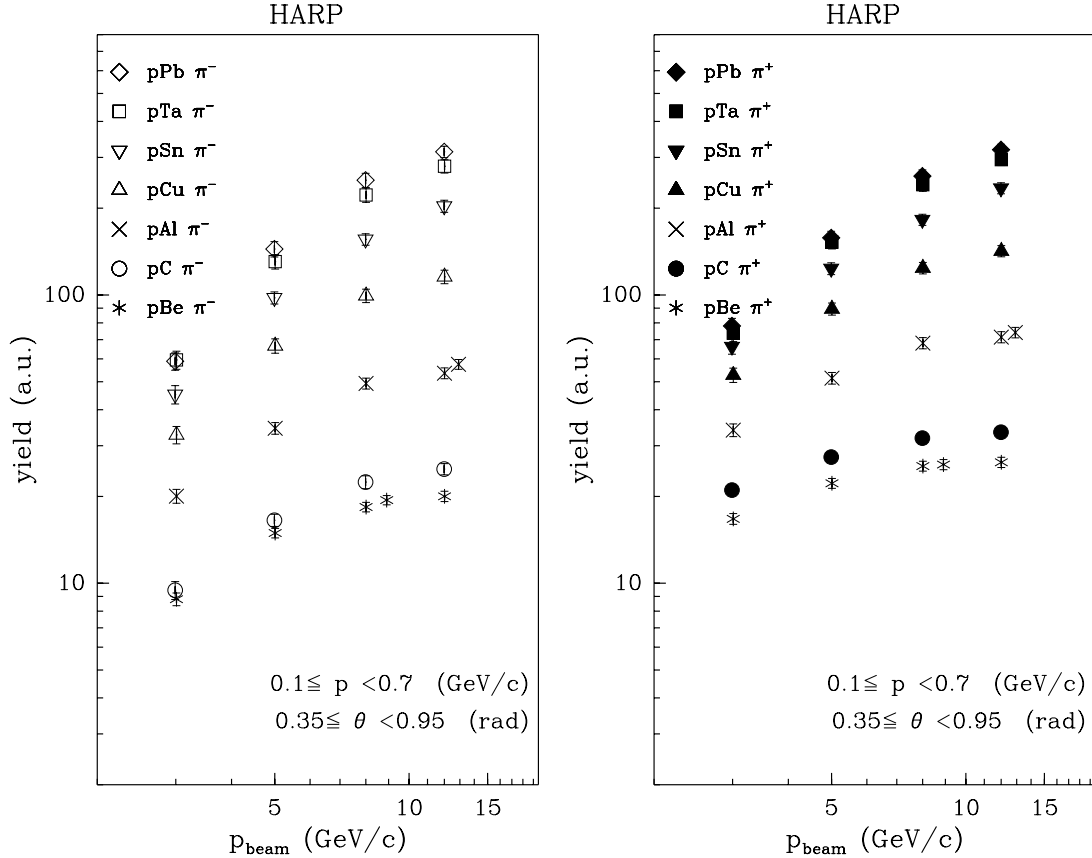


Fig. 6. The dependence on the beam momentum of the π^- (left) and π^+ (right) production yields in p -Be, p -C, p -Al, p -Cu, p -Sn, p -Ta, p -Pb interactions integrated over the forward angular region ($0.350 \text{ rad} \leq \theta < 0.950 \text{ rad}$) and momentum ($100 \text{ MeV}/c \leq p < 700 \text{ MeV}/c$). The results are given in arbitrary units, with a consistent scale between the left and right panel. Data points for different target nuclei and equal momenta are slightly shifted horizontally with respect to each other to increase the visibility

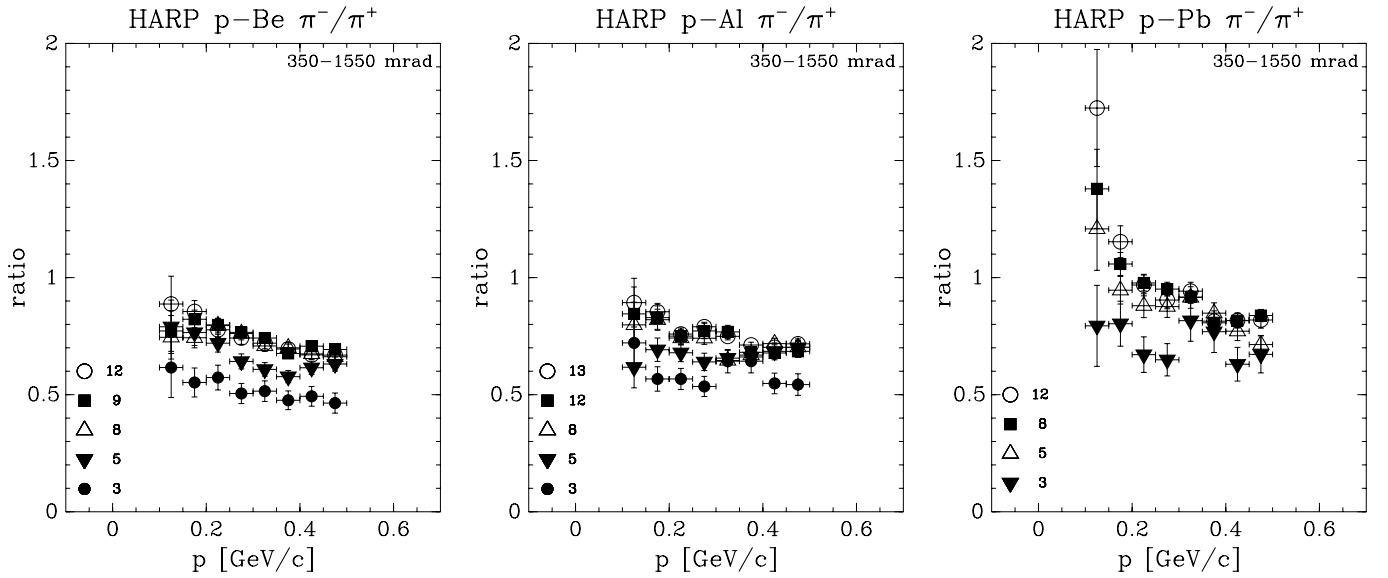


Fig. 7. The ratio of the differential cross-sections for π^- and π^+ production in p -Be (left panel), p -Al (middle panel) and p -Pb (right panel) interactions as a function of secondary momentum integrated over the forward angular region (shown in mrad). In the figure, the symbol legend 13 (9) refers to 12.9 (8.9) GeV/c nominal beam momentum

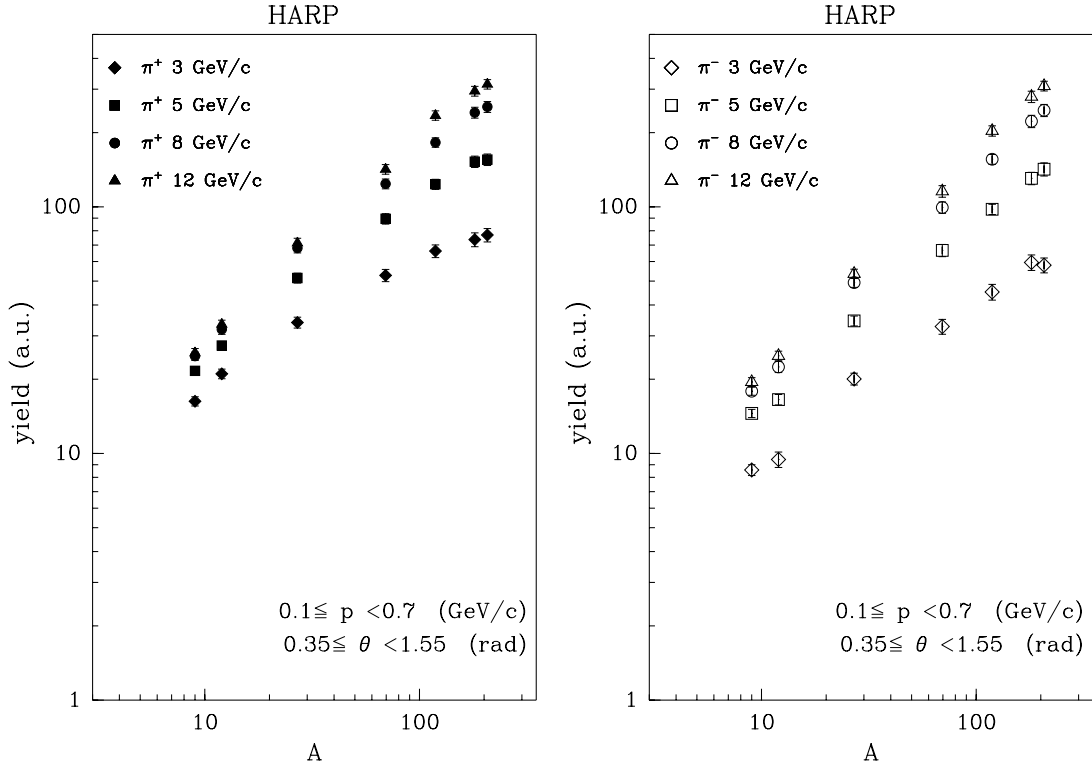


Fig. 8. The dependence on the atomic number A of the pion production yields in $p\text{-Be}$, $p\text{-C}$, $p\text{-Al}$, $p\text{-Cu}$, $p\text{-Sn}$, $p\text{-Ta}$, $p\text{-Pb}$ interactions integrated over the forward angular region ($0.350 \text{ rad} \leq \theta < 1.550 \text{ rad}$) and momentum ($100 \text{ MeV}/c \leq p < 700 \text{ MeV}/c$). The results are given in arbitrary units, with a consistent scale between the *left* and *right panel*. The vertical scale used in this figure is consistent with the one in Fig. 6

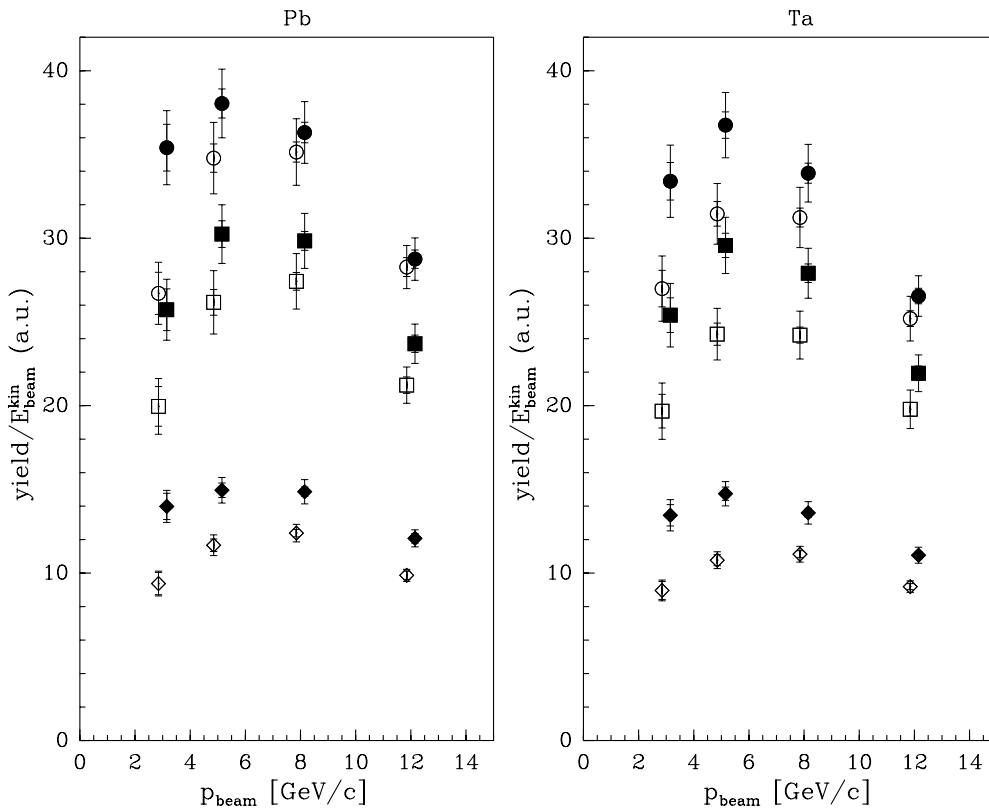


Fig. 9. The integrated yields normalized to the kinetic energy of the proton of the π^+ (closed symbols) and π^- (open symbols) yield as a function of incident proton beam momentum. Shown are the yields for lead (left) and tantalum (right). The *circles* indicate the integral over the full HARP acceptance (in the forward direction), the *squares* are integrated over $0.35 \text{ rad} < \theta < 0.95 \text{ rad}$, while the *diamonds* are calculated for the restricted angular range and $250 \text{ MeV}/c < p < 500 \text{ MeV}/c$. The *full error bar* shows the overall (systematic and statistical) error, while the *inner error bar* shows the error relevant for the point-to-point comparison. For the latter error only the uncorrelated systematic uncertainties were added to the statistical error

Table 2. Experimental uncertainties for the beryllium, aluminium and lead analyses. The numbers represent the uncertainty in percent of the cross-section integrated over the angle and momentum region indicated. The overall normalization has an uncertainty of 2% for Be and Al and 3% for Pb, and is not reported in the table

p (GeV/c)		0.1–0.3		0.3–0.5		0.5–0.7			
Angle (mrad)		350– 950	950– 1550	1550– 2150	350– 950	950– 1550	1550– 2150	350– 950	950– 1550
3 GeV/c									
Total syst.	(Be)	11.6	4.6	2.6	3.6	7.5	10.5	9.6	16.4
	(Al)	9.9	5.1	3.5	3.9	7.7	12.9	10.0	14.4
	(Pb)	11.7	6.8	6.3	3.7	5.9	6.4	11.0	14.7
Statistics	(Be)	4.5	3.8	4.9	3.5	5.9	16.0	4.7	13.0
	(Al)	4.0	3.3	4.2	3.2	5.1	11.3	4.2	9.9
	(Pb)	5.8	4.6	5.5	4.8	6.8	14.1	6.7	13.4
5 GeV/c									
Total syst.	(Be)	11.0	4.7	2.7	3.9	4.8	7.8	6.5	11.4
	(Al)	9.9	5.0	3.5	3.9	5.0	6.8	8.5	12.2
	(Pb)	12.4	7.4	6.3	4.0	5.2	6.8	6.8	11.3
Statistics	(Be)	2.2	1.8	2.3	1.4	2.2	4.5	1.7	3.5
	(Al)	2.7	2.4	3.0	2.1	3.2	6.3	2.5	5.2
	(Pb)	2.8	2.3	2.8	2.2	2.9	5.2	2.7	4.6
8 GeV/c									
Total syst.	(Be)	10.8	5.2	3.1	5.1	3.9	6.8	6.7	11.3
	(Al)	9.6	5.2	3.6	4.1	4.3	7.2	7.3	11.4
	(Pb)	11.1	7.4	6.4	4.2	4.7	6.6	6.6	9.3
Statistics	(Be)	1.7	1.4	1.8	1.1	1.7	3.2	1.2	2.5
	(Al)	1.6	1.5	1.9	1.2	1.9	3.6	1.4	2.7
	(Pb)	1.5	1.3	1.6	1.1	1.6	2.7	1.3	2.2
8.9 GeV/c									
Total syst.	(Be)	8.8	4.4	2.7	4.5	4.0	7.8	7.4	12.3
Statistics	(Be)	1.1	1.0	1.3	0.8	1.2	2.4	0.9	1.8
12 GeV/c									
Total syst.	(Be)	10.7	5.1	2.9	4.3	3.8	6.7	6.6	11.1
	(Al)	9.8	5.8	4.1	3.9	4.5	6.8	7.5	10.8
	(Pb)	10.8	7.1	6.7	2.9	4.4	5.6	7.1	9.1
Statistics	(Be)	1.6	1.4	1.7	1.0	1.5	2.9	1.1	2.2
	(Al)	1.9	1.9	2.4	1.5	2.2	4.4	1.6	3.2
	(Pb)	2.1	1.9	2.4	1.7	2.4	4.3	2.0	3.4
12.9 GeV/c									
Total syst.	(Al)	9.7	5.4	3.8	3.7	4.1	6.7	7.3	11.1
Statistics	(Al)	0.7	0.6	0.8	0.5	0.8	1.4	0.6	1.0

hemisphere ($100 \text{ MeV}/c < p < 700 \text{ MeV}/c$ and $0.35 < \theta < 1.55$). The results are shown in Fig. 9. The integrated yields normalized to the kinetic energy of the incoming beam particles are shown for Pb in the left panel and compared with the Ta data in the right panel. The outer error bars indicate the total statistical and systematic errors. If one compares the π^+ and π^- rates for a given beam momentum or if one compares the rates at a different beam momentum the relative systematic error is reduced by about a factor two. The relative uncertainties are shown as inner error bar. It is shown that in our kinematic coverage the optimum yield is between 5 GeV/c and 8 GeV/c. To show the trend the rates within restricted ranges are also given: a restricted angular range ($0.35 < \theta < 0.95$) and a range further restricted in momentum ($250 \text{ MeV}/c < p <$

$500 \text{ MeV}/c$). The latter range may be most representative for the neutrino factory. One notes that the Pb and Ta data yield the same conclusions. Although the units are indicated as “arbitrary”, for the largest region, the yield is expressed as $d^2\sigma/dpd\Omega$ in mb/(GeV/c sr). For the other regions the same normalization is chosen, but now scaled with the relative bin size to show visually the correct ratio of number of pions produced in these kinematic regions.

Of course this analysis only gives a simplified picture of the results. One should note that the best result can be obtained by using the full information of the double-differential cross-section and by developing designs optimized specifically for each single beam momentum. Then these optimized designs can be compared.

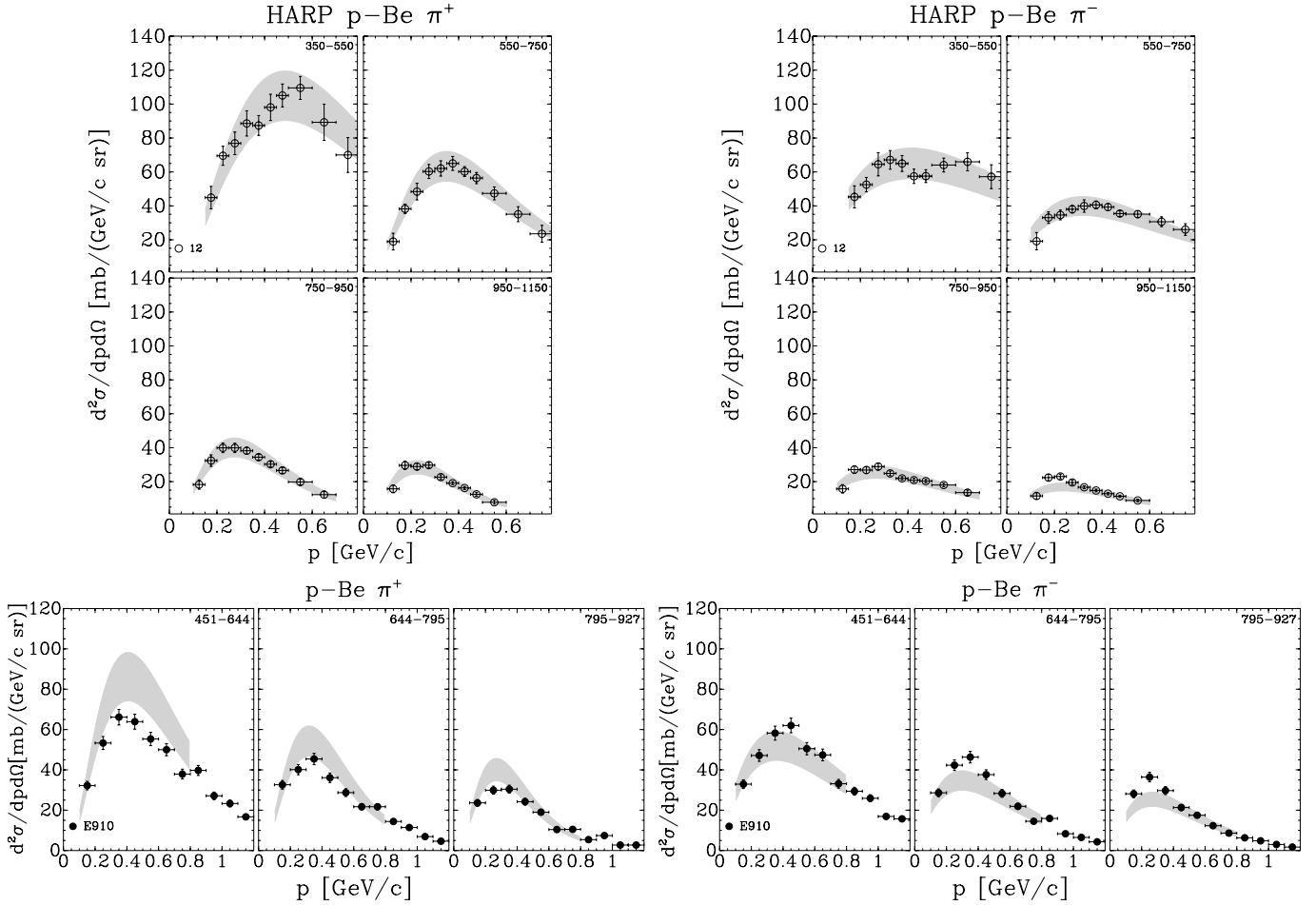


Fig. 10. Comparison of the HARP Be data with π^+ and π^- production data from [16] taken with 12.3 GeV/c protons. The top panels show a parametrization of the π^+ (left) and π^- (right) production data described in this paper. The data have been normalized to represent $d^2\sigma/\text{dpd}\Omega$. The shaded band represents the area between two parametrizations which contain the data points. The bottom panels show the comparison of the same parametrization, now binned according to the E910 data. The bottom left (right) panel shows the π^+ (π^-) production data of [16]. The angular regions are indicated in mrad in the upper right-hand corner of each plot

3.2 Comparisons with earlier data

Available data to be compared with are very scarce and in general suffer from large systematic and statistical uncertainties, except for the following two examples.

The p -Be data at 12.3 GeV/c from the E910 experiment [16] are in reasonable agreement with our results as shown in Fig. 10. In order to take into account the different angular binnings which prevent a direct comparison, a Sanford-Wang parametrization [42] is fitted to our data. The fit is performed to the data redefined as $d^2\sigma/\text{dpd}\Omega$. As the Sanford-Wang parametrization does not fit perfectly our data, a $\pm 15\%$ band which contains fully our experimental data points has been chosen for the comparison as shown in Fig. 10(top panels). The same parametrizations are then displayed in the binning of E910. While the shape of the distributions are similar for both π^+ and π^- in the HARP and E910 data sets, the absolute cross-sections disagree by up to 15% for the π^+ data and agree well for the π^- data. (The parametrization shows similar difficulties to

fit both π^- data sets). One should note that the range of the systematic errors of the HARP data is 5% to 10% and similar for the E910 data, such that the disagreement is not much larger than one standard deviation. The difference in the π^+/π^- ratio between the two experiments is about 15%, which is more significant given the expected correlations between the uncertainties in the measurements of the π^+ and π^- spectra. This effect may point to an underestimation of systematic effects on the absolute normalization, efficiencies or background subtractions. Owing to the symmetry of the HARP TPC, including its trigger counter, we do not expect a large systematic error in the HARP data between π^+ and π^- production cross-sections.⁴

Our p -Al data have been compared with π^+ and π^- production measurements at 12 GeV/c incident proton momentum from Shibata et al. [17]. Their data were

⁴ As a side remark, E910 data shows a step around 800 MeV/c in momentum (inverse for π^+ , π^-) that may explain also the observed discrepancy.

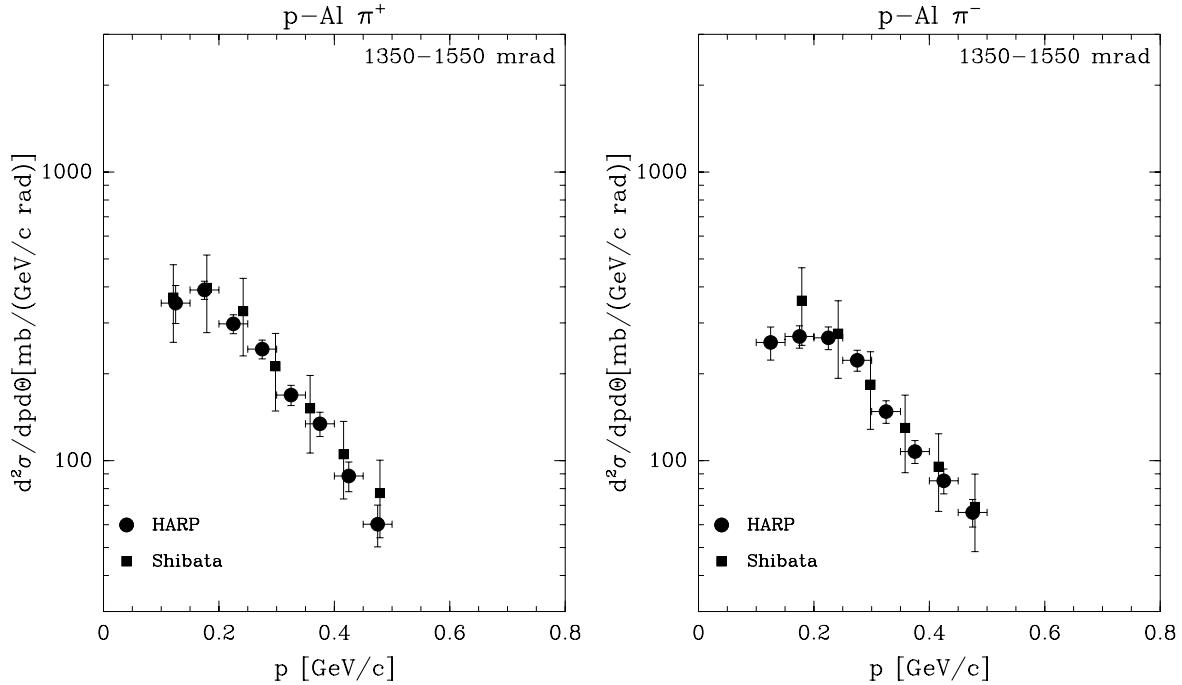


Fig. 11. Comparison of HARP p -Al data with π^+ and π^- production data at 90° from [17] taken with 12 GeV/c incident protons. The left panel shows the comparison of the π^+ production data of [17] with the data reported here; the right panel shows instead the comparison with the π^- production data. The data sets compares well with our results (filled circles) in the angular region $1.35 \text{ rad} \leq \theta < 1.55 \text{ rad}$

taken with a magnetic spectrometer and only measurements at 90° from the initial proton direction are available. The statistical point-to-point errors are quoted to be 3%, while the overall normalization has a 30% uncertainty due to the knowledge of the acceptance. In Fig. 11 their data are shown together with the results reported in this paper. Their data set compares well with the data described in this paper (filled circles) in the angular region $1.35 \text{ rad} \leq \theta < 1.55 \text{ rad}$ at the same proton beam momentum.⁵

4 Summary and conclusions

The analysis of the production of charged pions at large angles with respect to the beam direction for protons of 3 GeV/c, 5 GeV/c, 8 GeV/c, 8.9 GeV/c (Be only), 12 GeV/c and 12.9 GeV/c (Al only) impinging on thin (5% nuclear interaction length) beryllium, aluminium and lead targets is presented. The secondary pion yields are measured in a large angular and momentum range and double-differential cross-sections are obtained. A detailed error estimation is discussed. Results on the dependence of

charged pion production on the target atomic number A are also presented.

The use of a single detector for a range of beam momenta makes possible to measure the dependence of the pion yield on the secondary particle momentum and emission angle θ with high precision. The A dependence of the cross-section can be studied using the combination of the present data with the data obtained with carbon, copper, tin [20] and tantalum [21] targets in the same experiment. The yields integrated over relatively large angular and momentum regions show a smooth trend in their A and beam-momentum dependence.

The data taken with the lead target is important for the design studies for a neutrino factory. These data show a similar behaviour as the previously reported data with a tantalum target.

Acknowledgements. We gratefully acknowledge the help and support of the PS beam staff and of the numerous technical collaborators who contributed to the detector design, construction, commissioning and operation. In particular, we would like to thank G. Barichello, R. Brocard, K. Burin, V. Carassiti, F. Chignoli, D. Conventi, G. Decreuse, M. Delattre, C. Detraz, A. Domeniconi, M. Dwuznik, F. Evangelisti, B. Friend, A. Iaciofano, I. Krasin, D. Lacroix, J.-C. Legrand, M. Lobello, M. Lollo, J. Loquet, F. Marinilli, R. Mazza, J. Mulon, L. Musa, R. Nicholson, A. Pepato, P. Petev, X. Pons, I. Rusinov, M. Scandurra, E. Usenko, and R. van der Vlugt, for their support in the construction of the detector. The collaboration acknowledges the major contributions and advice of M. Baldo-Ceolin, L. Linssen, M.T. Mu-

⁵ In this comparison data are compared with their proper experimental normalization factors, while in the previous published comparison of our carbon and copper target data with their data sets, normalization factors 0.72 (0.91) were used, still compatible with their overall quoted normalization uncertainty of 30%.

ciaccia and A. Pullia during the construction of the experiment. The collaboration is indebted to V. Ableev, P. Arce, F. Bergsma, P. Binko, E. Boter, C. Buttar, M. Calvi, M. Campanelli, C. Cavion, A. Chukanov, A. De Min, M. Doucet, D. Düllmann, R. Engel, V. Ermilova, W. Flegel, P. Gruber, Y. Hayato, P. Hodgson, A. Ichikawa, I. Kato, O. Klimov, T. Kobayashi, D. Kustov, M. Laveder, M. Mass, H. Meinhard, T. Nakaya, K. Nishikawa, M. Paganoni, F. Paleari, M. Pasquali, J. Pasternak, C. Pattison, M. Placentino, S. Robbins, G. Santin, S. Simone, A. Tornero, S. Troquereau, S. Ueda, A. Valassi, F. Vannucci and K. Zuber for their contributions to the experiment and to P. Dini for his contribution to MC production.

We acknowledge the contributions of V. Ammosov, G. Chelkov, D. Dedovich, F. Dydak, M. Gostkin, A. Gusakov, D. Kharichenko, V. Koreshev, Z. Kroumchtein, I. Nefedov, A. Semak, J. Wotschack, V. Zaets and A. Zhemchugov to the work described in this paper.

The experiment was made possible by grants from the Institut Interuniversitaire des Sciences Nucléaires and the In-

teruniversitair Instituut voor Kernwetenschappen (Belgium), Ministerio de Educacion y Ciencia, Grant FPA2003-06921-c02-02 and Generalitat Valenciana, grant GV00-054-1, CERN (Geneva, Switzerland), the German Bundesministerium für Bildung und Forschung (Germany), the Istituto Nazionale di Fisica Nucleare (Italy), INR RAS (Moscow) and the Particle Physics and Astronomy Research Council (UK). We gratefully acknowledge their support. This work was supported in part by the Swiss National Science Foundation and the Swiss Agency for Development and Cooperation in the framework of the programme SCOPES – scientific co-operation between eastern Europe and Switzerland.

Appendix: Cross-section data

See Tables 3–8.

Table 3. HARP results for the double-differential π^+ production cross-section in the laboratory system, $d^2\sigma\pi^+/(dpd\theta)$ for p -Be interactions. Each row refers to a different ($p_{\min} \leq p < p_{\max}$, $\theta_{\min} \leq \theta < \theta_{\max}$) bin, where p and θ are the pion momentum and polar angle, respectively. The central value as well as the square-root of the diagonal elements of the covariance matrix are given. The overall normalization has an uncertainty of 2%, and is not reported in the table

θ_{\min} (rad)	θ_{\max} (rad)	p_{\min} (GeV/c)	p_{\max} (GeV/c)	$d^2\sigma\pi^+/(dpd\theta)$ (barn/(GeV/c rad))				
				3 GeV/c	5 GeV/c	8 GeV/c	12 GeV/c	12.9 GeV/c
0.35	0.55	0.15	0.20	0.063 ± 0.015	0.107 ± 0.017	0.121 ± 0.016	0.130 ± 0.015	0.126 ± 0.019
		0.20	0.25	0.090 ± 0.015	0.131 ± 0.014	0.161 ± 0.014	0.174 ± 0.014	0.195 ± 0.016
		0.25	0.30	0.104 ± 0.015	0.191 ± 0.023	0.199 ± 0.018	0.213 ± 0.018	0.215 ± 0.019
		0.30	0.35	0.151 ± 0.025	0.229 ± 0.021	0.236 ± 0.019	0.232 ± 0.022	0.248 ± 0.021
		0.35	0.40	0.178 ± 0.018	0.237 ± 0.016	0.237 ± 0.016	0.266 ± 0.018	0.245 ± 0.016
		0.40	0.45	0.163 ± 0.016	0.222 ± 0.014	0.254 ± 0.018	0.261 ± 0.014	0.275 ± 0.022
		0.45	0.50	0.187 ± 0.018	0.245 ± 0.020	0.281 ± 0.014	0.281 ± 0.019	0.294 ± 0.019
		0.50	0.60	0.185 ± 0.018	0.232 ± 0.016	0.274 ± 0.017	0.284 ± 0.018	0.307 ± 0.019
		0.60	0.70	0.117 ± 0.020	0.214 ± 0.022	0.285 ± 0.026	0.249 ± 0.024	0.250 ± 0.030
		0.70	0.80	0.083 ± 0.016	0.150 ± 0.029	0.208 ± 0.037	0.187 ± 0.029	0.196 ± 0.029
0.55	0.75	0.10	0.15	0.050 ± 0.016	0.076 ± 0.017	0.081 ± 0.018	0.092 ± 0.015	0.074 ± 0.019
		0.15	0.20	0.108 ± 0.016	0.111 ± 0.013	0.145 ± 0.012	0.132 ± 0.010	0.149 ± 0.011
		0.20	0.25	0.126 ± 0.019	0.171 ± 0.017	0.202 ± 0.014	0.197 ± 0.015	0.189 ± 0.019
		0.25	0.30	0.181 ± 0.020	0.218 ± 0.020	0.210 ± 0.017	0.218 ± 0.016	0.235 ± 0.016
		0.30	0.35	0.167 ± 0.020	0.214 ± 0.016	0.212 ± 0.014	0.220 ± 0.015	0.242 ± 0.018
		0.35	0.40	0.179 ± 0.017	0.196 ± 0.013	0.217 ± 0.014	0.222 ± 0.013	0.253 ± 0.016
		0.40	0.45	0.156 ± 0.015	0.183 ± 0.013	0.224 ± 0.012	0.209 ± 0.010	0.235 ± 0.011
		0.45	0.50	0.139 ± 0.013	0.175 ± 0.011	0.206 ± 0.011	0.211 ± 0.011	0.220 ± 0.013
		0.50	0.60	0.103 ± 0.013	0.149 ± 0.013	0.185 ± 0.013	0.179 ± 0.014	0.185 ± 0.015
		0.60	0.70	0.050 ± 0.014	0.102 ± 0.016	0.130 ± 0.018	0.131 ± 0.017	0.137 ± 0.017
0.75	0.95	0.10	0.15	0.079 ± 0.017	0.067 ± 0.013	0.079 ± 0.013	0.087 ± 0.013	0.089 ± 0.013
		0.15	0.20	0.121 ± 0.017	0.143 ± 0.015	0.162 ± 0.012	0.157 ± 0.012	0.157 ± 0.016
		0.20	0.25	0.136 ± 0.017	0.173 ± 0.016	0.193 ± 0.015	0.191 ± 0.013	0.193 ± 0.014
		0.25	0.30	0.125 ± 0.014	0.167 ± 0.012	0.188 ± 0.012	0.197 ± 0.013	0.193 ± 0.013
		0.30	0.35	0.120 ± 0.014	0.146 ± 0.012	0.175 ± 0.011	0.192 ± 0.012	0.185 ± 0.009
		0.35	0.40	0.103 ± 0.012	0.150 ± 0.011	0.171 ± 0.009	0.175 ± 0.008	0.167 ± 0.009
		0.40	0.45	0.078 ± 0.009	0.129 ± 0.010	0.146 ± 0.009	0.137 ± 0.007	0.147 ± 0.008
		0.45	0.50	0.072 ± 0.009	0.096 ± 0.010	0.126 ± 0.007	0.121 ± 0.006	0.129 ± 0.008
		0.50	0.60	0.044 ± 0.008	0.065 ± 0.008	0.097 ± 0.009	0.095 ± 0.008	0.096 ± 0.009
		0.60	0.70	0.021 ± 0.006	0.039 ± 0.007	0.059 ± 0.010	0.058 ± 0.010	0.060 ± 0.010

Table 7. HARP results for the double-differential π^+ production cross-section in the laboratory system, $d^2\sigma\pi^+/(dpd\theta)$ for p -Pb interactions. Each row refers to a different ($p_{\min} \leq p < p_{\max}$, $\theta_{\min} \leq \theta < \theta_{\max}$) bin, where p and θ are the pion momentum and polar angle, respectively. The central value as well as the square-root of the diagonal elements of the covariance matrix are given. The overall normalization has an uncertainty of 3%, and is not reported in the table

θ_{\min} (rad)	θ_{\max} (rad)	p_{\min} (GeV/c)	p_{\max} (GeV/c)	$d^2\sigma\pi^+/(dpd\theta)$ (barn/(GeV/c rad))			
				3 GeV/c	5 GeV/c	8 GeV/c	12 GeV/c
0.35	0.55	0.15	0.20	0.34 ± 0.12	0.80 ± 0.21	1.14 ± 0.32	1.49 ± 0.40
		0.20	0.25	0.29 ± 0.09	0.95 ± 0.16	1.86 ± 0.24	1.80 ± 0.26
		0.25	0.30	0.48 ± 0.11	1.26 ± 0.13	2.09 ± 0.14	2.42 ± 0.26
		0.30	0.35	0.75 ± 0.11	1.25 ± 0.11	1.99 ± 0.15	2.75 ± 0.26
		0.35	0.40	0.56 ± 0.08	1.31 ± 0.13	2.19 ± 0.16	2.69 ± 0.17
		0.40	0.45	0.53 ± 0.07	1.43 ± 0.11	2.21 ± 0.13	2.33 ± 0.14
		0.45	0.50	0.56 ± 0.10	1.29 ± 0.09	2.04 ± 0.11	2.32 ± 0.16
		0.50	0.60	0.45 ± 0.07	1.22 ± 0.09	2.07 ± 0.13	2.22 ± 0.16
		0.60	0.70	0.22 ± 0.05	0.84 ± 0.12	1.73 ± 0.20	2.03 ± 0.21
		0.70	0.80	0.12 ± 0.03	0.52 ± 0.09	1.09 ± 0.19	1.52 ± 0.22
0.55	0.75	0.10	0.15	0.21 ± 0.11	0.66 ± 0.24	0.93 ± 0.35	0.91 ± 0.41
		0.15	0.20	0.47 ± 0.11	1.25 ± 0.17	1.81 ± 0.21	2.14 ± 0.30
		0.20	0.25	0.70 ± 0.12	1.23 ± 0.13	2.11 ± 0.18	3.03 ± 0.24
		0.25	0.30	0.88 ± 0.12	1.37 ± 0.13	2.26 ± 0.15	2.89 ± 0.19
		0.30	0.35	0.53 ± 0.07	1.12 ± 0.09	2.09 ± 0.15	2.62 ± 0.16
		0.35	0.40	0.55 ± 0.07	0.95 ± 0.09	2.09 ± 0.14	2.68 ± 0.22
		0.40	0.45	0.58 ± 0.07	1.03 ± 0.10	1.86 ± 0.10	2.69 ± 0.15
		0.45	0.50	0.54 ± 0.08	1.02 ± 0.07	1.63 ± 0.09	2.38 ± 0.13
		0.50	0.60	0.27 ± 0.06	0.74 ± 0.08	1.30 ± 0.09	1.78 ± 0.16
		0.60	0.70	0.16 ± 0.03	0.42 ± 0.06	0.89 ± 0.11	1.21 ± 0.14
0.75	0.95	0.10	0.15	0.44 ± 0.13	0.90 ± 0.22	1.21 ± 0.31	1.27 ± 0.35
		0.15	0.20	0.77 ± 0.11	1.55 ± 0.14	2.16 ± 0.15	2.54 ± 0.21
		0.20	0.25	0.86 ± 0.10	1.37 ± 0.13	2.27 ± 0.14	2.93 ± 0.24
		0.25	0.30	0.70 ± 0.09	1.22 ± 0.13	2.02 ± 0.13	2.75 ± 0.18
		0.30	0.35	0.54 ± 0.07	1.05 ± 0.08	1.85 ± 0.12	2.22 ± 0.15
		0.35	0.40	0.40 ± 0.05	0.96 ± 0.07	1.60 ± 0.10	2.09 ± 0.13
		0.40	0.45	0.41 ± 0.06	0.80 ± 0.06	1.39 ± 0.08	1.81 ± 0.11
		0.45	0.50	0.32 ± 0.05	0.67 ± 0.05	1.22 ± 0.07	1.52 ± 0.09
		0.50	0.60	0.18 ± 0.03	0.44 ± 0.05	0.83 ± 0.08	1.04 ± 0.10
		0.60	0.70	0.08 ± 0.02	0.25 ± 0.04	0.46 ± 0.07	0.63 ± 0.08
0.95	1.15	0.10	0.15	0.73 ± 0.18	1.01 ± 0.20	1.47 ± 0.26	1.52 ± 0.32
		0.15	0.20	0.82 ± 0.09	1.64 ± 0.12	2.19 ± 0.15	2.60 ± 0.21
		0.20	0.25	0.71 ± 0.10	1.37 ± 0.10	1.97 ± 0.12	2.82 ± 0.19
		0.25	0.30	0.73 ± 0.09	1.10 ± 0.10	1.60 ± 0.11	2.13 ± 0.16
		0.30	0.35	0.41 ± 0.07	0.80 ± 0.08	1.31 ± 0.10	1.73 ± 0.12
		0.35	0.40	0.29 ± 0.05	0.66 ± 0.06	1.11 ± 0.06	1.64 ± 0.11
		0.40	0.45	0.29 ± 0.05	0.61 ± 0.05	0.88 ± 0.05	1.23 ± 0.10
		0.45	0.50	0.20 ± 0.04	0.48 ± 0.05	0.66 ± 0.04	0.86 ± 0.08
		0.50	0.60	0.12 ± 0.02	0.23 ± 0.04	0.46 ± 0.04	0.53 ± 0.07
		0.60	0.70	0.05 ± 0.01	0.10 ± 0.02	0.25 ± 0.03	0.35 ± 0.05
1.15	1.35	0.10	0.15	0.79 ± 0.18	1.17 ± 0.23	1.82 ± 0.30	1.76 ± 0.34
		0.15	0.20	0.93 ± 0.10	1.51 ± 0.11	2.30 ± 0.14	2.53 ± 0.22
		0.20	0.25	0.65 ± 0.08	1.21 ± 0.09	1.86 ± 0.11	2.64 ± 0.20
		0.25	0.30	0.51 ± 0.07	0.91 ± 0.08	1.41 ± 0.10	1.84 ± 0.17
		0.30	0.35	0.33 ± 0.05	0.59 ± 0.06	0.94 ± 0.08	1.17 ± 0.09
		0.35	0.40	0.23 ± 0.04	0.38 ± 0.04	0.74 ± 0.05	0.93 ± 0.07
		0.40	0.45	0.17 ± 0.03	0.29 ± 0.03	0.55 ± 0.04	0.72 ± 0.07
		0.45	0.50	0.11 ± 0.03	0.21 ± 0.03	0.37 ± 0.04	0.45 ± 0.06

Table 7. continued

θ_{\min} (rad)	θ_{\max} (rad)	p_{\min} (GeV/c)	p_{\max} (GeV/c)	3 GeV/c	$d^2\sigma^{\pi^+}/(dpd\theta)$ (barn/(GeV/c rad))		
					5 GeV/c	8 GeV/c	12 GeV/c
1.35	1.55	0.10	0.15	0.85 ± 0.17	1.44 ± 0.29	1.84 ± 0.39	2.03 ± 0.41
		0.15	0.20	0.94 ± 0.10	1.41 ± 0.12	2.21 ± 0.15	2.50 ± 0.19
		0.20	0.25	0.71 ± 0.08	0.96 ± 0.08	1.57 ± 0.11	1.84 ± 0.14
		0.25	0.30	0.38 ± 0.06	0.64 ± 0.06	1.04 ± 0.08	1.48 ± 0.12
		0.30	0.35	0.22 ± 0.04	0.43 ± 0.04	0.74 ± 0.05	0.87 ± 0.08
		0.35	0.40	0.11 ± 0.03	0.35 ± 0.04	0.53 ± 0.04	0.63 ± 0.06
		0.40	0.45	0.04 ± 0.01	0.23 ± 0.03	0.38 ± 0.03	0.46 ± 0.05
		0.45	0.50	0.04 ± 0.01	0.15 ± 0.02	0.22 ± 0.03	0.28 ± 0.04
1.55	1.75	0.10	0.15	0.66 ± 0.15	1.37 ± 0.23	1.54 ± 0.30	2.03 ± 0.40
		0.15	0.20	0.70 ± 0.09	1.40 ± 0.11	1.93 ± 0.13	2.27 ± 0.18
		0.20	0.25	0.53 ± 0.07	0.99 ± 0.07	1.34 ± 0.09	1.42 ± 0.11
		0.25	0.30	0.26 ± 0.06	0.58 ± 0.06	0.87 ± 0.06	0.95 ± 0.08
		0.30	0.35	0.13 ± 0.03	0.41 ± 0.04	0.53 ± 0.04	0.66 ± 0.06
		0.35	0.40	0.10 ± 0.03	0.26 ± 0.03	0.36 ± 0.03	0.47 ± 0.05
		0.40	0.45	0.06 ± 0.02	0.16 ± 0.03	0.25 ± 0.02	0.31 ± 0.04
		0.45	0.50	0.04 ± 0.01	0.09 ± 0.02	0.15 ± 0.02	0.17 ± 0.03
1.75	1.95	0.10	0.15	0.64 ± 0.14	1.03 ± 0.19	1.31 ± 0.20	1.72 ± 0.29
		0.15	0.20	0.66 ± 0.07	1.14 ± 0.09	1.64 ± 0.09	1.85 ± 0.13
		0.20	0.25	0.36 ± 0.05	0.74 ± 0.06	1.02 ± 0.07	1.10 ± 0.10
		0.25	0.30	0.18 ± 0.04	0.34 ± 0.05	0.63 ± 0.05	0.56 ± 0.06
		0.30	0.35	0.08 ± 0.02	0.17 ± 0.03	0.34 ± 0.04	0.36 ± 0.05
		0.35	0.40	0.07 ± 0.02	0.10 ± 0.02	0.22 ± 0.03	0.18 ± 0.03
		0.40	0.45	0.05 ± 0.02	0.06 ± 0.01	0.14 ± 0.02	0.10 ± 0.02
		0.45	0.50	0.02 ± 0.01	0.03 ± 0.01	0.07 ± 0.02	0.07 ± 0.01
1.95	2.15	0.10	0.15	0.79 ± 0.15	0.83 ± 0.14	1.14 ± 0.18	1.46 ± 0.23
		0.15	0.20	0.65 ± 0.09	0.89 ± 0.08	1.17 ± 0.06	1.36 ± 0.11
		0.20	0.25	0.36 ± 0.07	0.51 ± 0.05	0.75 ± 0.05	1.04 ± 0.10
		0.25	0.30	0.15 ± 0.05	0.28 ± 0.05	0.45 ± 0.05	0.40 ± 0.07
		0.30	0.35	0.05 ± 0.02	0.14 ± 0.03	0.20 ± 0.03	0.19 ± 0.03
		0.35	0.40	0.03 ± 0.02	0.09 ± 0.02	0.09 ± 0.01	0.13 ± 0.02
		0.40	0.45	0.02 ± 0.01	0.04 ± 0.01	0.06 ± 0.01	0.09 ± 0.02
		0.45	0.50	0.01 ± 0.01	0.02 ± 0.01	0.04 ± 0.01	0.07 ± 0.02

Table 8. HARP results for the double-differential π^- production cross-section in the laboratory system, $d^2\sigma^{\pi^-}/(dpd\theta)$ for p–Pb interactions. Each row refers to a different ($p_{\min} \leq p < p_{\max}$, $\theta_{\min} \leq \theta < \theta_{\max}$) bin, where p and θ are the pion momentum and polar angle, respectively. The central value as well as the square-root of the diagonal elements of the covariance matrix are given. The overall normalization has an uncertainty of 3%, and is not reported in the table

θ_{\min} (rad)	θ_{\max} (rad)	p_{\min} (GeV/c)	p_{\max} (GeV/c)	3 GeV/c	$d^2\sigma^{\pi^-}/(dpd\theta)$ (barn/(GeV/c rad))		
					5 GeV/c	8 GeV/c	12 GeV/c
0.35	0.55	0.15	0.20	0.17 ± 0.09	0.58 ± 0.22	1.59 ± 0.36	1.92 ± 0.47
		0.20	0.25	0.33 ± 0.11	0.89 ± 0.18	2.00 ± 0.27	2.66 ± 0.31
		0.25	0.30	0.25 ± 0.06	0.98 ± 0.12	2.07 ± 0.14	2.54 ± 0.24
		0.30	0.35	0.49 ± 0.11	0.96 ± 0.11	1.99 ± 0.13	2.30 ± 0.16
		0.35	0.40	0.37 ± 0.08	0.88 ± 0.09	1.63 ± 0.09	2.09 ± 0.12
		0.40	0.45	0.30 ± 0.06	0.92 ± 0.07	1.63 ± 0.08	2.04 ± 0.13
		0.45	0.50	0.31 ± 0.06	0.79 ± 0.06	1.48 ± 0.07	1.89 ± 0.13
		0.50	0.60	0.34 ± 0.06	0.78 ± 0.06	1.38 ± 0.08	1.50 ± 0.14
0.60	0.70	0.21	0.05	0.64 ± 0.07	1.37 ± 0.10	1.32 ± 0.12	
		0.70	0.80	0.11 ± 0.04	0.45 ± 0.08	1.06 ± 0.15	1.46 ± 0.15

Table 8. continued

θ_{\min} (rad)	θ_{\max} (rad)	p_{\min} (GeV/c)	p_{\max} (GeV/c)	3 GeV/c	$d^2\sigma\pi^-/(dpd\theta)$ (barn/(GeV/c rad))	5 GeV/c	8 GeV/c	12 GeV/c
1.75	1.95	0.10	0.15	0.72 ± 0.15	1.13 ± 0.20	1.78 ± 0.25	2.36 ± 0.44	
		0.15	0.20	0.52 ± 0.07	1.09 ± 0.09	1.44 ± 0.07	1.84 ± 0.12	
		0.20	0.25	0.32 ± 0.06	0.65 ± 0.06	0.92 ± 0.06	1.10 ± 0.10	
		0.25	0.30	0.11 ± 0.03	0.36 ± 0.04	0.56 ± 0.05	0.58 ± 0.05	
		0.30	0.35	0.11 ± 0.03	0.25 ± 0.03	0.30 ± 0.03	0.41 ± 0.05	
		0.35	0.40	0.09 ± 0.03	0.15 ± 0.03	0.23 ± 0.02	0.31 ± 0.03	
		0.40	0.45	0.07 ± 0.03	0.11 ± 0.02	0.20 ± 0.02	0.30 ± 0.04	
		0.45	0.50	0.04 ± 0.02	0.09 ± 0.02	0.14 ± 0.02	0.21 ± 0.04	
1.95	2.15	0.10	0.15	0.69 ± 0.14	1.08 ± 0.20	1.52 ± 0.20	1.84 ± 0.31	
		0.15	0.20	0.43 ± 0.07	0.84 ± 0.07	1.11 ± 0.06	1.35 ± 0.10	
		0.20	0.25	0.23 ± 0.05	0.40 ± 0.06	0.68 ± 0.05	0.90 ± 0.10	
		0.25	0.30	0.08 ± 0.03	0.21 ± 0.03	0.42 ± 0.04	0.51 ± 0.06	
		0.30	0.35	0.05 ± 0.02	0.11 ± 0.03	0.24 ± 0.03	0.34 ± 0.06	
		0.35	0.40	0.03 ± 0.02	0.07 ± 0.01	0.17 ± 0.02	0.19 ± 0.03	
		0.40	0.45	0.02 ± 0.02	0.08 ± 0.02	0.12 ± 0.02	0.14 ± 0.03	
		0.45	0.50	0.02 ± 0.02	0.08 ± 0.02	0.08 ± 0.01	0.09 ± 0.02	

References

1. HARP Collaboration, M.G. Catanesi et al., CERN-SPSC/99-35 (1999)
2. A. Blondel et al., CERN-2004-002, ECFA/04/230
3. M.M. Alsharoa et al., Phys. Rev. ST Accel. Beams **6**, 081001 (2003)
4. G. Battistoni, Nucl. Phys. B Proc. Suppl. **100**, 101 (2001)
5. T. Stanev, Rapporteur's talk at the 26th Int. Cosmic Ray Conference, Salt Lake City, Utah, USA, ed. by B.L. Dingus et al., AIP Conf. Proc. **516**, 247 (2000)
6. T.K. Gaisser, Nucl. Phys. B Proc. Suppl. **87**, 145 (2000)
7. R. Engel, T.K. Gaisser, T. Stanev, Phys. Lett. B **472**, 113 (2000)
8. M. Honda, Nucl. Phys. B **77**, 140 (1999)
9. K2K Collaboration, M.H. Ahn et al., Phys. Rev. Lett. **90**, 041801 (2003)
10. K2K Collaboration, M.H. Ahn et al., Phys. Rev. D **74**, 072003 (2006) [arXiv:hep-ex/0606032]
11. The MiniBooNE Collaboration, A.A. Aguilar-Arevalo, arXiv:0704.1500
12. BooNe Collaboration, E. Church et al., FERMILAB-PROPOSAL-0898 (1997)
13. SciBooNE Collaboration, A.A. Aguilar-Arevalo et al., FERMILAB-PROPOSAL-0954 (2006) [arXiv:hep-ex/0601022]
14. P.A. Piroué, A.J.S. Smith, Phys. Rev. **148**, 1315 (1966)
15. S. Boyarinov et al., Sov. J. Nucl. Phys. **46**, 871 (1987)
16. E910 Collaboration, I. Chemakin et al., Phys. Rev. C **65**, 024904 (2002)
17. T.-A. Shibata et al., Nucl. Phys. A **408**, 525 (1983)
18. HARP Collaboration, M.G. Catanesi et al., Eur. Phys. J. C **52**, 29 (2007) [arXiv:hep-ex/0702024]
19. HARP Collaboration, M.G. Catanesi et al., Nucl. Phys. B **732**, 1 (2006) [arXiv:hep-ex/0510039]
20. HARP Collaboration, M.G. Catanesi et al., accepted for publication on Eur. Phys. J. C [arXiv:0709.3464]
21. HARP Collaboration, M.G. Catanesi et al., Eur. Phys. J. C **51**, 787 (2007) [arXiv:0706.1600]
22. HARP Collaboration, M.G. Catanesi et al., submitted to JINST [arXiv:0709.1600]
23. HARP Collaboration, M.G. Catanesi et al., Nucl. Instrum. Methods A **571**, 527 (2007)
24. HARP Collaboration, M.G. Catanesi et al., Nucl. Instrum. Methods A **571**, 564 (2007)
25. M. Anfreville et al., Nucl. Instrum. Methods A **481**, 339 (2002)
26. M. Baldo-Ceolin et al., Nucl. Instrum. Methods A **532**, 548 (2004)
27. M. Bonesini et al., IEEE Trans. Nucl. Sci. **50**, 1053 (2003)
28. E. Radicioni, IEEE Trans. Nucl. Sci. **52**, 2986 (2005)
29. M. Bogomilov et al., Nucl. Instrum. Methods A **508**, 152 (2003)
30. G. Barr et al., Nucl. Instrum. Methods A **533**, 214 (2004)
31. M. Bogomilov et al., IEEE Trans. Nucl. Sci. **54**, 342 (2007)
32. L. Durieu, A. Mueller, M. Martini, PAC-2001-TPAH142, Presented at IEEE Particle Accelerator Conference (PAC2001), Chicago, Illinois, 18–22 June 2001
33. L. Durieu et al., Proceedings of PAC'97, Vancouver, 1997
34. L. Durieu, O. Fernando, CERN PS/PA Note 96-38
35. G. D'Agostini, Nucl. Instrum. Methods A **362**, 487 (1995)
36. GEANT4 Collaboration, S. Agostinelli et al., Nucl. Instrum. Methods A **506**, 250 (2003)
37. R.C. Fernow, J. Gallardo, private communication
38. S.J. Brooks, private communication
39. S.J. Brooks, K.A. Walaton, Nucl. Phys. B Proc. Suppl. **155**, 295 (2006)
40. K. Long, Nucl. Phys. B Proc. Suppl. **154**, 111 (2006)
41. K. Long, ISS/2005/01, http://www.hep.ph.ic.ac.uk/iss/issnotes/ISS_Doc1_v02_13-7-2005.pdf
42. J.R. Sanford, C.L. Wang, AGS internal report (Brookhaven National Laboratory, 1967) unpublished